


Three-fragment dissociation of $C_2H_2^{2+}$ and $C_2H_2^{3+}$ produced by slow- Ar^{8+} -ion impactT. Jiang,^{1,2} B. Wang,^{1,2} Y. Zhang,^{1,2} L. Wei,³ S. Chen,^{1,2} W. Yu,^{1,2} Y. Zou,^{1,2} L. Chen,^{1,2} and B. Wei^{1,2,*}¹*Institute of Modern Physics, Fudan University, Shanghai 200433, China*²*Key Laboratory of Nuclear Physics and Ion-Beam Application (MOE), Fudan University, Shanghai 200433, China*³*School of Nuclear Science and Technology, Lanzhou 730000, China* (Received 20 December 2018; revised manuscript received 22 March 2019; published 16 August 2019)

Three-fragment dissociation dynamics of $C_2H_2^{2+}$ dications and $C_2H_2^{3+}$ trications induced by electron capture of slow (3-keV/u) Ar^{8+} ions are investigated. Using cold target recoil ion momentum spectroscopy, the complete kinematic information and thus kinetic energy releases are determined for the three-fragment channels, $C_2H_2^{2+} \rightarrow H^+ + C_2^+ + H$ and $C_2H_2^{3+} \rightarrow H^+ + C_2^+ + H^+$. Then by analyzing the complete kinematics with a Dalitz plot and Newton diagram, different fragmentations, i.e., concerted or sequential pathway, are identified. For dications, the sequential fragmentation $C_2H_2^{2+} \rightarrow H^+ + C_2H^+ \rightarrow H^+ + C_2^+ + H$ is dominant. However, the trications mainly dissociate via the synchronous concerted fragmentation. The sequential pathway $C_2H_2^{3+} \rightarrow H^+ + C_2H^{2+} \rightarrow H^+ + C_2^+ + H^+$, which was found to be significant at higher collision velocities, is not observed here. This distinction reveals the important role of projectile velocity on the fragmentation dynamics for some specific channels.

DOI: [10.1103/PhysRevA.100.022705](https://doi.org/10.1103/PhysRevA.100.022705)**I. INTRODUCTION**

Fragmentation of organic hydrocarbon molecules plays a role in various areas such as astrophysics [1,2] and fusion plasmas [3]. When exposed to an external field, electrons in polyatomic molecules may be excited to higher states, which then undergo electronic decays simultaneously coupled with ultrafast nuclear rearrangement, resulting in complicated dynamical patterns, e.g., isomerization, sequential dissociation, and multifragment channels [4–10]. These experiments exhibit increasing complexity with the rising size of the molecule system due to more electronic states involved, which still presents a challenge to experimental investigations.

With the help of well-established imaging techniques, in particular, the advent of cold target recoil ion momentum spectroscopy (COLTRIMS) [11], ionic fragments can be detected in coincidence, and thus the fragmentation dynamics can be reconstructed. Acetylene is one of the smallest organic molecules with notable complexities. It contains seven basic normal modes of vibration, both σ and π bonding, and the isomerized vinylidene CCH_2 has a few kcal/mol barriers higher [12]. For that, acetylene has drawn great attention to recent subjects of ion- and laser-induced experiments. A number of fragmentation channels have been studied in a wide variety of laser, electron, and ion-acetylene interactions, and corresponding dynamics have been reconstructed in different energy ranges to unravel the proton migration and/or fragmentation mechanism of acetylene in ionic forms [8–10,13–18]. Previously the three-body fragmentation mechanisms (sequential and concerted breakup) of linear triatomic molecular ions of, e.g., CO_2^{3+} [19–21] and OCS^{3+} [22], have been clearly disentangled. However, corresponding investigations

are scarce on the doubly or triply charged C_2H_2 molecule, especially in the slow highly charged ion (HCI) collisions. Flammini *et al.* investigated three fragmentation channels of acetylene dications leading to $C_2H^+ + H^+$, $C_2^+ + H^+$, and $C^+ + H^+$ induced by 4-keV electron impact and found that the excess energy of parent dications fragmenting into $C_2^+ + H^+$ is mainly transferred to the second step of the sequential dissociation [7]. Using a near single-cycle pulse, Burger *et al.* mainly investigated the three-body paths, $H^+ + C_2^+ + H^+$ and $H^+ + C^+ + CH^+$, to observe the evolution of proton isomerization in acetylene dications [8]. In 30-keV/u Ar^{8+} experiments, De *et al.* identified the decay processes of multicharged C_2H_2 and reported the diatomiclike behavior of C_2 complex in those processes [9]. Mizuno *et al.* found that the kinetic energy release (KER) strongly depends on charge-changing type in two-body fragmentation pathways of C_2H_2 dications by fast-heavy ion (2 MeV Si^{2+}) impact and reported that the mean KERs are much smaller than those in photoionization experiments [10]. In a very recent study of 50 keV/u Ne^{8+} in collision with neutral C_2H_2 , Xu *et al.* found that in addition to the concerted and sequential breakup, fragmentation mechanisms associated to different vibrational modes made significant contributions to the $H^+ + C_2^+ + H^+$ fragmentation path [18].

To provide complementary information on fragmentation dynamics of multiply charged C_2H_2 , we investigate in the present work three-body fragmentation of C_2H_2 dications and trications induced by slow (3 keV/u) Ar^{8+} impact. Using the COLTRIMS, we have determined the complete kinematics for two channels, $C_2H_2^{2+} \rightarrow H^+ + C_2^+ + H$ and $C_2H_2^{3+} \rightarrow H^+ + C_2^+ + H^+$. By analyzing the kinetic energy release, the Dalitz plot, and Newton diagram [19,23] corresponding to each dissociation channel, we have identified fragmentation pathways, i.e., concerted or sequential processes. In the case of $C_2H_2^{3+}$, a different fragmentation dynamics was

*Corresponding author: brwei@fudan.edu.cn

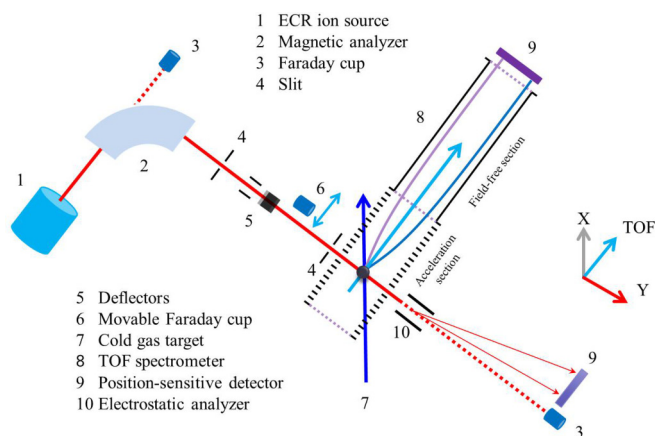


FIG. 1. Schematic of the highly charged ion collision platform.

observed compared to that obtained in collisions with fast ions [18]. This distinction will be discussed in light of ionization mechanism of molecules in both slow and fast ion impact experiments.

II. EXPERIMENTAL SETUP

The experiment was conducted on the highly charged ion collision platform at Fudan University in Shanghai. The composition of the platform has been described earlier [24]. As shown in Fig. 1, it mainly consists of a permanent-magnet 14.5-GHz electron cyclotron resonance (ECR) ion source and a COLTRIMS setup. Briefly, the beam of highly charged ions Ar^{8+} was extracted from the ion source, focused by an einzel lens, and postaccelerated to 3 keV/u. After the charge-state selection by a 90° magnetic analyzer, the ion beam passed through a slit, two deflectors (horizontal and vertical deflectors), and a second slit along the beam line. The current of the undeflected ion beams was measured by the Faraday cup placed behind the magnetic analyzer along the axis of the incident beam. The current of the selected ions was measured using a movable Faraday cup which could be placed between the deflectors and the second slit. Finally, the ion beam was guided into the COLTRIMS chamber and collected by a third Faraday cup along the beam line when the voltages of the electrostatic analyzer were turned off.

Details about the COLTRIMS setup have also been given elsewhere [23,25–27]. The gas of C_2H_2 at a pressure of 2 bar passed through a $30\text{-}\mu\text{m}$ nozzle and three skimmers, leading to the formation of a cold supersonic jet. The gas jet was injected along the vertical axis in the interaction chamber where high vacuum was maintained at $\sim 2.8 \times 10^{-8}$ Torr. The selected highly charged ion beam of diameter less than 1 mm crossed perpendicularly the cold target jet, where collisions between the projectile ions Ar^{8+} and C_2H_2 molecules occurred. During a single collision event, depending on the impact parameter, the incident highly charged ion could capture one or more electrons from the target and might deposit excitation energy in the target. The charged intact molecule or fragments due to dissociation of the molecular ion were extracted and accelerated in an electrostatic field of 50 V/cm along the axis of the time-of-flight (TOF) spectrometer. After

flying through the acceleration section of 10 cm in length and a field-free section of 20 cm, the recoil ions were detected by a position-sensitive detector (PSD, 80 mm in diameter). The time and position information of each charged recoil fragment was used afterward to reconstruct the three-dimensional momenta of the fragment. Usually in a multielectron (two, three, or more) capture process, the electrons captured by the highly charged projectile ion occupied excited orbitals. The scattered projectile ion temporarily in a multiply excited state might lose one or more electrons via autoionization in a time range of picosecond. The stabilized scattered projectile ion then passed through an electrostatic analyzer, which was composed of two parallel plates of 120 mm length separated by a distance of 30 mm. In the present experiment, scattered projectile ions of Ar^{7+} and Ar^{6+} were dominant, while a small amount of stable Ar^{5+} ions were observed. One meter after the deviation by the analyzer, the ions were detected by another position-sensitive detector. When the potential difference between the two parallel plates was applied to 410 V, the incident ion beam Ar^{8+} was moved out of the PSD and the distance between Ar^{7+} and Ar^{6+} was 13.2 mm on the PSD. To record the coincidence information of each collision event, the scattered ion signal was used as the common start for the time to digital converter (TDC), and the recoil ion signals were used as stop(s). To exclude the random events from the true coincidence events, the intensity of the incident ion beam was reduced to maintain a low coincidence count rate of $\sim 200/\text{s}$. Furthermore, for a three-body channel in which all fragments were detected, the random coincidence events, if there were any, could be further excluded through applying the momentum conservation constraint.

III. RESULTS AND DISCUSSION

TOF spectra due to 3-keV/u Ar^{8+} impact on C_2H_2 molecules were recorded in coincidence with Ar^{7+} and Ar^{6+} as shown in Figs. 2(a) and 2(b), respectively. In Fig. 2(a), the narrow peaks of stable C_2H_2^+ and $\text{C}_2\text{H}_2^{2+}$ are dominant, which originated from single electron capture and double electron capture with the loss of one electron leading to the scattered projectile Ar^{7+} . The width of C_2H_2^+ corresponds to a kinetic energy dispersion of about tens of meV, which is related to the kinetic energy dispersion of neutral molecules from the supersonic jet and to the recoil energy dispersion gained during the collision in one electron capture process. This small value reflects the coldness of the gas target. The kinetic energy dispersion of neutral molecules is therefore negligible in the analyses of dissociation of multiply charged molecules. The narrow peak of $\text{C}_2\text{H}_2^{2+}$ is also present in Fig. 2(b), which originated from double electron capture with the stabilization of the two captured electrons. It is notable that the most intense peak of C_2H_2^+ in Fig. 2(a) is completely absent in Fig. 2(b). This shows that double collision could be neglected in the experiment. The intact singly and doubly charged parent ions were stable during the extraction time, showing that they were formed in long-distance gentle collisions without enough energy deposition during the interaction with the projectile ions. $^{13}\text{CCH}_2^+$ ions resulting from the ionization of ^{13}C -based molecules are also observed in Fig. 2(a), and the count of the corresponding peak is about 2% of that of

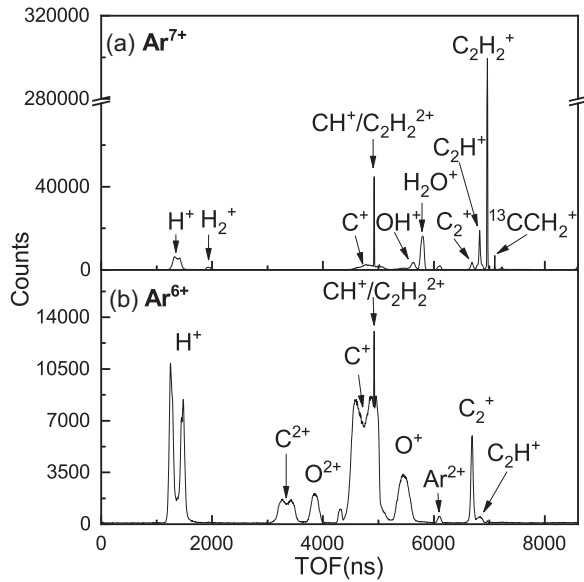


FIG. 2. TOF spectra of ions resulting from the dissociation of $\text{C}_2\text{H}_2^{r+}$ caused by 3-keV/u Ar^{8+} impact taken in coincidence with the (a) Ar^{7+} and (b) Ar^{6+} projectiles.

C_2H_2^+ , which is about twice the abundance of the isotope ^{13}C , since there are two carbon atoms in the acetylene molecule. The peak of C_2H^+ in both spectra might originate from two different two-fragment processes, i.e., $\text{C}_2\text{H}_2^+ \rightarrow \text{C}_2\text{H}^+ + \text{H}$ or $\text{C}_2\text{H}_2^{2+} \rightarrow \text{C}_2\text{H}^+ + \text{H}^+$. A small peak of C_2^+ is observed in both spectra. This ion is the characteristic indicator of a three-fragment process. Ions due to impurity Ar, H_2 , and H_2O are also observed in the spectrum of Figs. 2(a) and 2(b). Apart from H^+ , fragments associated to more than two-fragment processes such as C_2^+ and C^+ are observed in both spectra. Doubly charged atomic ions C^{2+} are observed only in Fig. 2(b), which are attributed to complete dissociation of the molecules, i.e., four-fragment processes, of highly charged

molecular ions. It could be noted that H^+ , C^+ , and C^{2+} present double peaks in the spectra. This is due to the fact that the collection efficiency of fast atomic ions with velocity perpendicular to the extraction field was relatively weak under the present experimental conditions, while ions with initial velocity along the extraction field towards or backward of the TOF tube were detected with higher efficiency, leading to the typical double peak in the spectra.

Although the molecule is small, the TOF spectra in Fig. 2 show very rich fragmentation schemes. Since the neutral fragments cannot be detected, the dissociation channels involving C^+ and C^{2+} will not be discussed here. Other two-fragment channels of $\text{C}_2\text{H}_2^{2+}$ dications, such as $\text{H}^+ + \text{C}_2\text{H}^+$, $\text{CH}^+ + \text{CH}^+$, and the isomerization channel $\text{C}^+ + \text{CH}_2^+$, have been studied in another paper [28]. In the following, we will focus our attention on three-fragment processes involving C_2^+ produced in the dissociation of $\text{C}_2\text{H}_2^{2+}$ and $\text{C}_2\text{H}_2^{3+}$.

Small regions of the ion-ion TOF map in coincidence respectively with the detection of Ar^{7+} and Ar^{6+} are shown in Fig. 3. Each collision event was plotted in the map, with the TOF of the heavy fragment along the vertical axis and the TOF of the light fragment along the horizontal axis. The ion pair $\text{H}^+ + \text{C}_2\text{H}^+$ resulting from the two-fragment dissociation of $\text{C}_2\text{H}_2^{2+}$ is observed in both spectra. The straight segment with a slope of 45° is characteristic of the momentum conservation in two-fragment dissociations. It is noticed that the spots of the $\text{H}^+ + \text{C}_2\text{H}^+$ pair with special shapes are very different from those of the $\text{H}^+ + \text{C}_2\text{H}^+$ pair. In coincidence with the detection of Ar^{7+} , the corresponding coincidence islands consist of two parts: an inclined straight segment [region A in Fig. 3(a)] and two circlelike spots [region B in Fig. 3(a)] around the nominal TOF of C_2^+ on both sides of the segment. In coincidence with the detected Ar^{6+} ion, the corresponding coincidence islands consist of only two circlelike spots distributed closely to the reference red line of zero slope, which means the momentum of the C_2^+ is almost zero. Taking into account of the linear symmetrical

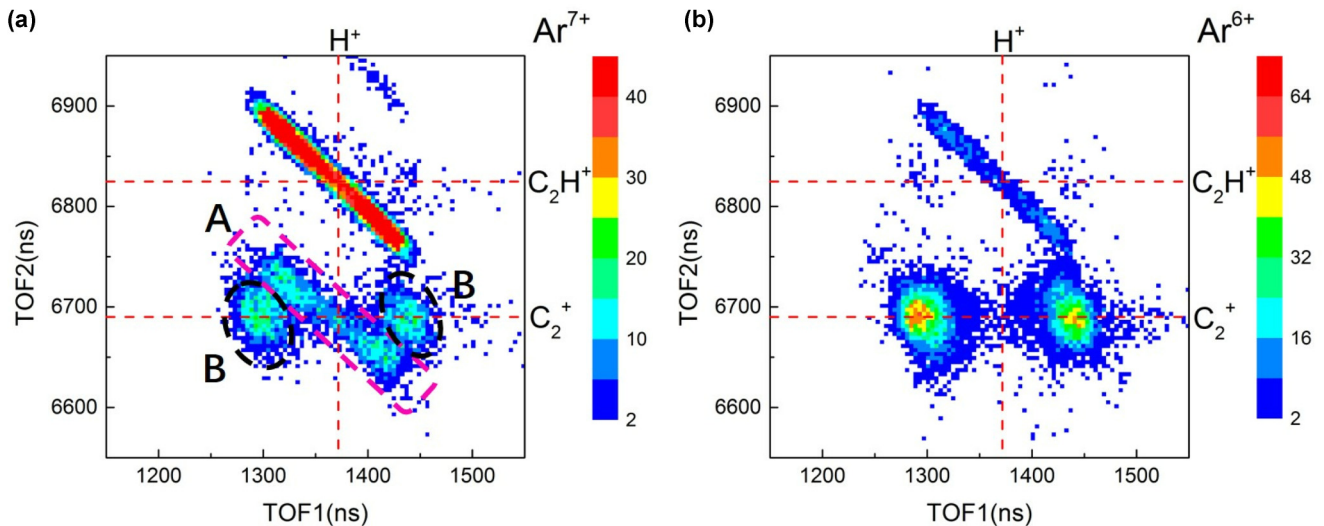


FIG. 3. Ion-ion coincidence TOF map resulting from the $\text{C}_2\text{H}_2^{r+}$ ($r = 2, 3$) dissociation caused by 3-keV/u Ar^{8+} impact taken in coincidence with the (a) Ar^{7+} and (b) Ar^{6+} projectiles. The red dotted lines parallel to the axes are the reference lines to mark the coinciding ions.

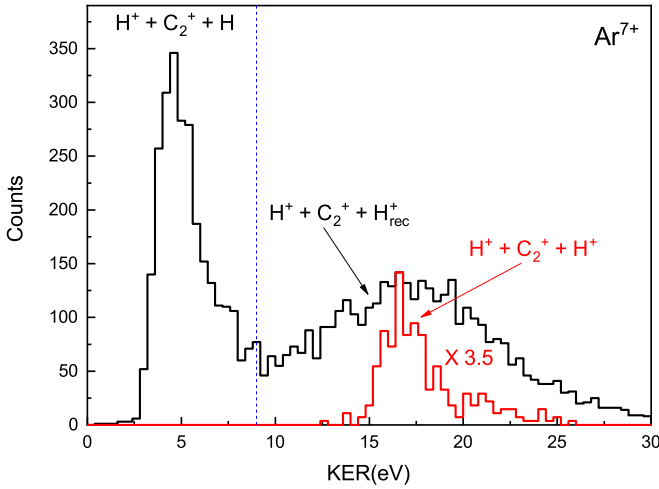


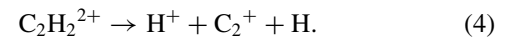
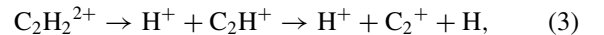
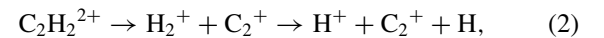
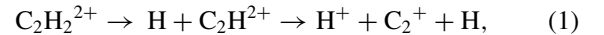
FIG. 4. Black line: KER distribution of the three-fragment process $C_2H_2^{2+} \rightarrow H^+ + C_2^+ + H$ and $C_2H_2^{3+} \rightarrow H^+ + C_2^+ + H_{rec}^+$. Red line: KER distribution for $C_2H_2^{3+} \rightarrow H^+ + C_2^+ + H^+$ where three fragments were all detected.

structure of the molecule, a possible mechanism to produce an immobile fragment of the central part C_2^+ could be the simultaneous loss of two H^+ from $C_2H_2^{3+}$ that the two H^+ fly oppositely with equal momenta. $C_2H_2^{3+}$ could be produced in a three-electron capture process in which one or two captured electrons were lost from the scattered projectile by autoionization, leading to Ar^{6+} or Ar^{7+} . The inclined segment for the ion pair $H^+ + C_2^+$ between the two circular spots in the coincidence map with Ar^{7+} presents a quite similar shape as a typical two-charged-fragment process shown by the spot of the ion pair $H^+ + C_2H^+$. This suggests that this part of the spot $H^+ + C_2^+$ corresponds most probably to the dissociation $C_2H_2^{2+} \rightarrow H^+ + C_2^+ + H$ involving two charged fragments, with the third one being neutral H . The count of the above three-fragment processes was measured to be not less than 5% of the count of all dissociations. Due to the poor collection efficiency of fast fragment ions with velocity perpendicular to the axis of the TOF tube, a part of the three-fragment events, notably those with the parent molecules aligned perpendicular to the TOF tube or with a large angle from the TOF tube, were not detected. Fortunately, for events where the angle between the flying direction of the light fragment H^+ and the TOF tube was less than 30° , complete dissociation dynamic pictures could be drawn from the detection of ionic fragments.

To get more information on the proposed three-fragment processes $C_2H_2^{3+} \rightarrow H^+ + C_2^+ + H^+$ and $C_2H_2^{2+} \rightarrow H^+ + C_2^+ + H$, the KER ($KER = \sum p_i^2/2m_i$) values were analyzed. According to the standard COLTRIMS methodology, the three-dimensional momenta of each detected ion, H^+ or C_2^+ , were determined from the TOF and the position of the ion on the PSD. Then the momenta of the third undetected fragment H or H^+ were reconstructed by applying momentum conservation under the assumption that the momenta of the parent ions $C_2H_2^{2+}$ or $C_2H_2^{3+}$ were zero. The KERs for these three-fragment processes were obtained as shown in Fig. 4. Two features are noticed in the KER distribution. The first one is a narrow peak at ~ 4.3 eV, corresponding

to region A in Fig. 3(a), which is attributed to the dissociation $C_2H_2^{2+} \rightarrow H^+ + C_2^+ + H$. And the second one is a broad component centered at a much higher kinetic energy of ~ 16.4 eV, which corresponds to region B in Fig. 3(a) and is tentatively attributed to the three-body dissociation of $C_2H_2^{3+}$ trications. However, in the present experiment, one of the protons in most cases was lost for the $H^+ + C_2^+ + H^+$ channel. This was mainly due to the low detection efficiency of multiple coincidence and the electronics dead time (~ 100 ns) preventing the second arriving proton from being detected. In order to explain the broad component, we first analyzed the rare events where three charged fragments were all detected, i.e., C_2^+ and two protons. The count of such events was about 16% of the total count of the $H^+ + C_2^+$ ion pairs. The KER distribution for the $H^+ + C_2^+ + H^+$ channel can be directly deduced using the measured momenta of the three fragments and is shown in Fig. 4 (the red line). This narrow peak centered also at 16.4 eV is in good agreement with the data reported in Ref. [18]. From the measured momenta of the three fragments, we can deduce the momenta of the parent ions. The obtained momentum of $C_2H_2^{3+}$ along each direction was found to be a broadened distribution around zero, which we attribute to the momentum measurement resolution of the COLTRIMS. Therefore, the momentum distribution of parent ions can drastically affect the estimation of the momentum distribution of the third undetected ionic fragment, resulting in the broadening of the KER distribution for $C_2H_2^{3+} \rightarrow H^+ + C_2^+$ with one proton undetected. To check this speculation, using the detected $H^+ + C_2^+ + H^+$ data, we have intentionally ignored one of the two detected protons and reconstructed its momentum employing the law of momentum conservation under the approximation of still parent ions. The obtained KER distribution was found to be much broader than the red line and very similar to the black line in Fig. 4. Therefore, we can infer that the broad component in Fig. 4 originates from the three-fragment dissociation of $C_2H_2^{3+}$ but with one undetected proton, here labeled as the channel $H^+ + C_2^+ + H_{rec}^+$.

For the three-fragment process $C_2H_2^{2+} \rightarrow H^+ + C_2^+ + H$, four possible pathways could be considered as follows:



For process (1), the first step would lead to the production of C_2H^{2+} . The presence or not of C_2H^{2+} ions in the spectra of Fig. 2 is hard to analyze, because the TOF of this ion is imbedded in the broad backward peak of C^+ . For searching C_2H^{2+} , we have constructed a TOF spectrum for events where only one ion was detected so that events containing C^+ were excluded. In this spectrum, the peak expected for C_2H^{2+} was not observed. Therefore, we deduce that for $C_2H_2^{2+}$, the channel of losing H^+ should be more likely than the channel of losing H . In the competition of the loss of H^+ and H , the process $C_2H_2^{2+} \rightarrow H^+ + C_2H^+$ is the main dissociation

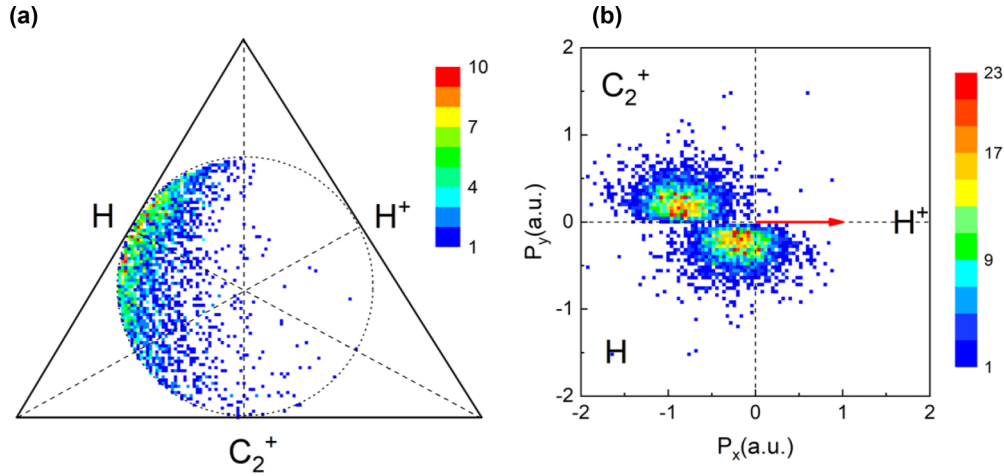


FIG. 5. (a) Dalitz plot and (b) Newton diagram for the three-fragment process $C_2H_2^{2+} \rightarrow H^+ + C_2^+ + H$ for the KER range of 2–9 eV.

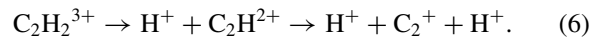
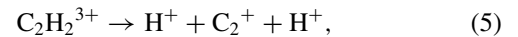
channel, while the process $C_2H_2^{2+} \rightarrow H + C_2H^{2+}$ is negligible. Based on this analysis, we consider that the contribution of process (1) should be excluded. For the first step of the process (2), although the peak of H_2^+ is observed in the TOF spectrum (Fig. 2), in the ion-ion coincidence TOF map, the ion pair $H_2^+ + C_2^+$ was not found due to the relatively small cross section [29]. In this work, the H_2^+ ions were mostly generated by the ionization of impurity H_2 from the background. So, if there is contribution of process (2), it should be rather low. In contrary to process (1), the first step of process (3) is demonstrated clearly by the spot of the ion pair $H^+ + C_2H^+$ in Fig. 3 and the peak of C_2H^+ in Fig. 2. So process (3) seems to be a possible channel to explain the three-fragment dissociation, $C_2H_2^{2+} \rightarrow H^+ + C_2^+ + H$.

To get more dynamical information on the three-fragment dissociation of $C_2H_2^{2+}$ involving H^+ , C_2^+ , and H and to identify the responsible process, the Dalitz plot and Newton diagram for events in the KER range of 2–9 eV were constructed and shown in Fig. 5. Dalitz plots and Newton diagrams are powerful tools to visualize the momentum correlation of fragments in a three-fragment process [30] and thus to identify the fragmentation mechanism [19,23]. They have been described in earlier work [23–27]. Briefly, in the Dalitz plot shown in Fig. 5(a), each edge of the equilateral triangle represents one fragment in the process, i.e., H^+ , C_2^+ , and H. The distance of a data point from the three edges equals the value $\varepsilon_i = p_i^2 / \sum p_i^2$ (where p_i is the momentum of fragment i). The momentum of neutral fragment H is very small, and the momenta of C_2^+ and H^+ are almost equal to each other. In process (2), the neutral fragment H and H^+ should gain comparable momenta. This would lead to a spot around the vertical middle line in the Dalitz plot. However, in Fig. 5(a), such a spot is not observed, confirming that the contribution of process (2) in the three-fragment process is negligible. In the two-step process (3), the $C_2H_2^{2+}$ dissociates into H^+ and C_2H^+ and then C_2H^+ releases the neutral fragment H while flying. In the first step, H^+ and C_2H^+ gain almost equal momenta. During the dissociation of C_2H^+ , H carries at least 4% of the momentum of C_2H^+ . The momentum of C_2^+ should be therefore slightly smaller than that of H^+ . In the synchronous concerted process (4), the neutral fragment H

plays a role of spectator and thus the two ionic fragments fly in nearly opposite directions due to Coulomb repulsion. For that, the momentum of neutral fragment H is much smaller than the momenta of C_2^+ and H^+ . For both (3) and (4) processes, the momenta of C_2^+ and H^+ are expected to be comparable, and the momentum of H is much smaller than the other fragments, both corresponding to the main feature of the Dalitz plot in Fig. 5(a).

In the Newton diagram, the momentum of H^+ is set as a unit in the positive direction of the x axis as the arrow shows in Fig. 5(b). The momenta of C_2^+ and neutral fragment H are set above and below the x axis, and the P_x and P_y represent the momenta parallel and vertical to the momentum of H^+ . In most events, the C_2^+ and neutral fragment H fly in the opposite direction of H^+ . Furthermore, the most probable momentum of H is small, and the angle between the momenta of H^+ and H has a wide distribution. Those features are more consistent with the kinematics of process (3) compared with those of process (4), since the angle between the momenta of corresponding fragments should be a particular value for a synchronous concerted process [31]. This finding is in accordance with previous pathway identifications made in the photo- and electron-impact double-ionization experiments [7,32]. Nevertheless, process (4) could also make a minor contribution to the three-fragment process.

For the acetylene trications $C_2H_2^{3+}$, they can also fragment via different pathways into $H^+ + C_2^+ + H^+$, including the concerted and sequential ones as follows:



The kinematics of the above two pathways has been differentiated and investigated in collisions with fast HCIs in Ref. [18]. In the present work, with slow HCI impact, we observed differences in the fragmentation dynamics. Figures 6(a) and 6(b) present the Dalitz plot and Newton diagram for the detected channel $C_2H_2^{3+} \rightarrow H^+ + C_2^+ + H^+$. We have also plotted the momentum correlation maps for the $C_2H_2^{3+} \rightarrow H^+ + C_2^+ + H_{rec}^+$ (not shown here), which presents similar main features as those of the detected

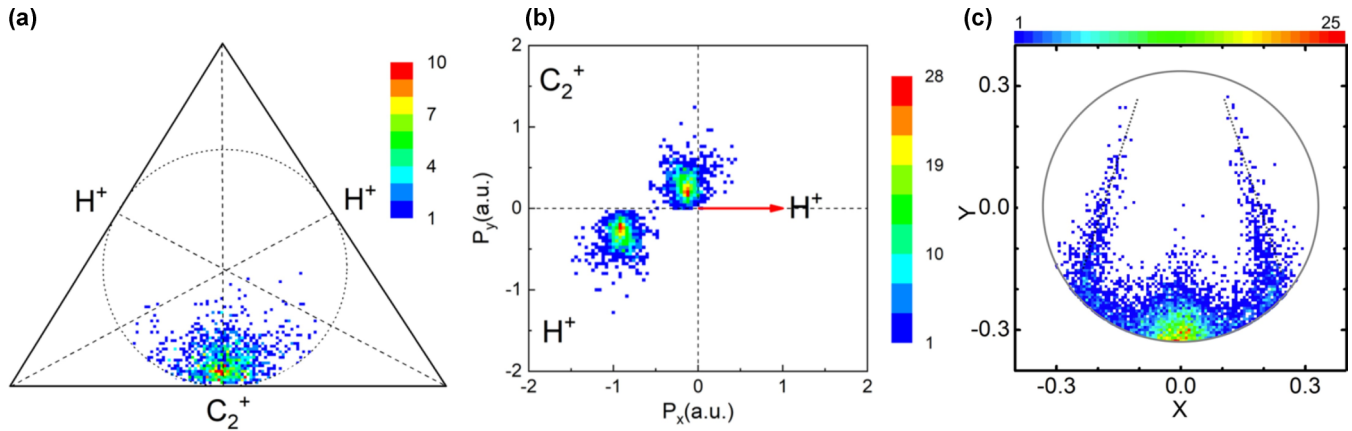


FIG. 6. (a) Dalitz plot and (b) Newton diagram for the three-fragment process $C_2H_2^{3+} \rightarrow H^+ + C_2^+ + H^+$ where three fragments were all detected. (c) Dalitz plot for $C_2H_2^{3+} \rightarrow H^+ + C_2^+ + H^+$ taken in the 50-keV/u Ne^{8+} collisions [18].

three-fragment channel (Fig. 6). In Fig. 6(a), most events gather around the perpendicular bisector of the C_2^+ edge, where the momentum of C_2^+ is distributed around zero and the momenta of two protons are nearly equal. From the Newton diagram shown in Fig. 6(b), we can see that not only are the momenta of the two H^+ ions very near, the angle between the two vectors is around 180° . These features provide more evidence for our previously proposed dissociation dynamics, i.e., the synchronous concerted fragmentation of $C_2H_2^{3+}$, in which the two protons break away initially with equal momentum from the two opposite sides of the linear molecule, leaving the inner C_2^+ nearly still [process (5)]. This channel, corresponding to the component of KER distribution centered at 16.4 eV, is therefore the common scheme observed in both slow and fast collisions [18]. The two-step sequential process (6) was found to give characteristic signatures in the Dalitz plot and Newton diagram, as shown clearly in the previous experiment with fast HCl impact [18]. In the 50-keV/u Ne^{8+} experiment [18], the sequential dissociation of $C_2H_2^{3+}$ trication is characterized by two notable findings: one is the distinct “horn” structure of the H^+ momentum in the Dalitz plot as shown in Fig. 6(c), which shows that one released H^+ takes much larger momentum than the other H^+ . The other is the opposite and equal momenta of the exploded C_2^+ and the second H^+ from the unstable $C_2H_2^{2+}$ illustrated in the Newton diagram (see Fig. 3(a) in Ref. [18]), which also shows the dynamical proof of the two-step dissociation mechanism. However, these features are totally absent in the present 3 keV/u Ar^{8+} experiment. In addition, the KER of the sequential process was determined as about 25 eV [18]. This high-energy component was not observed in our measured KER distribution (see Fig. 4). One may be concerned that the orientation of the acetylene could affect the analyses of observed dynamics. We could hardly collect the ionic fragments while the angle between the acetylene orientation and the direction of the projectile beam was less than 40° , which is due to the weakness of collection efficiency in the present experiment. In a recent theoretical study of 30 keV/u Ar^{8+} in collision with C_2H_2 [34], it was found that the sequential channels of $C_2H_2^{3+}$ exist only in the collision configuration where the acetylene orientation is perpendicular to the ion beam. From these analyses, we can infer that the sequential

channel [process (6)] is not likely to occur in the present experiment.

To understand the absence of the high-energy sequential channel in $C_2H_2^{3+}$ dissociation by 3 keV/u Ar^{8+} impact, we further analyzed the roles of the projectile velocity, charge redistribution, and delay time of $C_2H_2^{3+}$. In the most related 50-keV/u Ne^{8+} experiment [18], for the sequential channels of $C_2H_2^{3+}$, the kinetic energy of the first lost H^+ was measured to be around 20 eV, which is much larger than the energy of 8.2 eV of each H^+ exploded in the simultaneous loss process, and the second H^+ was released with a delay in time of less than half of the rotation period of the molecule, in the order of nanoseconds [33]. Knowing that this channel is opened in fast collisions, it could be related to the different ionization and excitation modes of the parent ion under different energy regions. In collisions between HCl and atomic or molecular targets, the velocity of HCl, $v_p = 1$ a.u., is a critical reference value. Collisions with $v_p \gg 1$ a.u. are classified as a swift interaction regime, where the projectile velocity is much larger than the velocities of the electrons occupying the outermost orbitals of the targets. In this region, the electron loss from the target could be induced by direct interaction with the HCl due to the very short collision time. In such cases, several electrons along the ion trajectory could be lost by the molecule, leading to the localized positive charge due to the ion impact. In the theoretical study of C_2H_2 molecules by 30-keV/u Ar^{8+} impact [34], it was found that the projectile distorts the electronic density to be strongly unbalanced, and then the interionic charge transfer before sequential dissociation lasts for more than 10 fs. As the first fast H^+ is also found to dissociate roughly in 10 fs, we can infer the electron distribution of the parent ion is not equilibrated before dissociation. For $C_2H_2^{3+}$, if the three positive charges are located at the same half side of the molecule due to swift impact of an HCl, stronger Coulombic repulsion between the proton and the adjacent doubly charged C is expected. This would lead to higher KER for the first escaping H^+ , while the second H in the near-neutral part of the residual molecule could not be lost simultaneously, as the charge distribution is more closed to balance. The delayed loss of the second H^+ could occur as soon as the charge is redistributed along the residual $C_2H_2^{2+}$ molecular chain. Collisions with $v_p < 1$ a.u.

are usually classified as a slow interaction regime. In this region, the ionized C_2H_2 have more time to approach equilibrium before dissociation. In the case of the C_2H_2 target by impact of slow HCl, the triply charged molecule could be expected to be prepared with a quasiequilibrium charge distribution after the transfer of three electrons, i.e., two protons at the two ends of the molecular chain and one positive charge at the center of the molecule. The Coulomb repulsion of the positive charges leads to the spontaneous break of the two C-H bonds, as what we observed in this experiment ($v_p = 0.34$ a.u.). In collisions at intermediate velocity regime, the characteristics of both slow and swift collisions should be expected; therefore the low KER synchronous concerted loss of $2H^+$ and the high KER sequential dissociation channel should coexist. This feature was observed in the experiment of Ref. [18] ($v_p = 1.4$ a.u.) with v_p slightly larger than the critical reference value. To get a better understanding of the relation between the fragmentation dynamics and the velocity of the incident ion, more experiments will be performed in the near future.

IV. CONCLUSIONS

On the highly charged ion collision platform, an experimental study of the three-fragment dissociation dynamics of $C_2H_2^{2+}$ and $C_2H_2^{3+}$ produced by slow Ar^{8+} -ion impact was conducted. With the COLTRIMS technique, the three-dimensional momenta of all fragments from each parent molecular ion were reconstructed and the KER was thus calculated. The KER distribution for the three-fragment process $C_2H_2^{2+} \rightarrow H^+ + C_2^+ + H$ was characterized by a peak at

around 4.3 eV, and that for the channel $C_2H_2^{3+} \rightarrow H^+ + C_2^+ + H^+$ was found to be centered at ~ 16.4 eV. Using a Dalitz plot and Newton diagram, we have analyzed the momentum correlation of fragments in each channel. We found that the sequential process $C_2H_2^{2+} \rightarrow H^+ + C_2H^+ \rightarrow H^+ + C_2^+ + H$ was dominant for the three-body breakup of acetylene dications. As for the trications, the major pathway was observed to be a synchronous concerted fragmentation, while the signature corresponding to the sequential pathway $C_2H_2^{3+} \rightarrow H^+ + C_2H^{2+} \rightarrow H^+ + C_2^+ + H^+$ was not found. Comparing to the previous experiment using faster HCl [18], we notice that for $C_2H_2^{3+}$ the synchronous concerted loss of two protons was the common dissociation scheme in both slow and fast collisions, whereas the sequential pathway present in fast collisions and absent in slow collisions seems to be very sensitive to the collision velocity. This indicates that the velocity of projectiles probably has a strong influence on the molecular fragmentation dynamics concerning the breakup pathways. In the near future, more experiments should be performed to understand the dependence of the fragmentation on the velocity of the incident ion.

ACKNOWLEDGMENTS

This work was supported by the National Key Research and Development Program of China under Grant No. 2017YFA0402300, the National Magnetic Confinement Fusion Program with Grant No. 2015GB117000, by the National Science Foundation of China under Contract No. 11674067, and by the Shanghai Leading Academic Discipline Project (Project No. B107).

-
- [1] M. R. Swain, G. Vasisht, and G. Tinetti, *Nature (London)* **452**, 329 (2008).
 - [2] R. Thissen, O. Witasse, O. Dutuit, C. S. Wedlund, G. Gronoff, and J. Liliensten, *Phys. Chem. Chem. Phys.* **13**, 18264 (2011).
 - [3] D. Reiter and R. K. Janev, *Contrib. Plasma Phys.* **50**, 986 (2010).
 - [4] T. Kinugawa, P. Lablanquie, F. Penent, J. Palaudoux, and J. H. D. Eland, *J. Electron. Spectrosc. Relat. Phenom.* **141**, 143 (2004).
 - [5] N. Saito, M. Nagoshi, M. Machida, I. Koyano, A. De Fanis, and K. Ueda, *Chem. Phys. Lett.* **393**, 295 (2004).
 - [6] S. J. King and S. D. Price, *J. Chem. Phys.* **127**, 174307 (2007).
 - [7] R. Flammini, M. Satta, E. Fainelli, and L. Avaldi, *Phys. Chem. Chem. Phys.* **13**, 19607 (2011).
 - [8] C. Burger, N. G. Kling, R. Siemering, A. S. Alnaser, B. Bergues, A. M. Azzeer, R. Moshhammer, R. de Vivie-Riedle, M. Kubel, and M. F. Kling, *Faraday Discuss.* **194**, 495 (2016).
 - [9] S. De, J. Rajput, A. Roy, P. N. Ghosh, and C. P. Safvan, *Phys. Rev. A* **77**, 022708 (2008).
 - [10] T. Mizuno and A. Itoh, *J. Phys.: Conf. Ser.* **488**, 012027 (2014).
 - [11] J. Ullrich, R. Moshhammer, A. Dorn, R. Dörner, L. P. H. Schmidt, and H. Schmidt-Böcking, *Rep. Prog. Phys.* **66**, 1463 (2003).
 - [12] K. M. Ervin, J. Ho, and W. C. Lineberger, *J. Chem. Phys.* **91**, 5974 (1989).
 - [13] T. Osipov, C. L. Cocke, M. H. Prior, A. Landers, T. Weber, O. Jagutzki, L. Schmidt, H. Schmidt-Böcking, and R. Dörner, *Phys. Rev. Lett.* **90**, 233002 (2003).
 - [14] Y. H. Jiang, A. Rudenko, O. Herrwerth, L. Foucar, M. Kurka, K. U. Kühnel, M. Lezius, M. F. Kling, J. van Tilborg, A. Belkacem, K. Ueda, S. Dusterer, R. Treusch, C. D. Schroter, R. Moshhammer, and J. Ullrich, *Phys. Rev. Lett.* **105**, 263002 (2010).
 - [15] E. Wells, C. E. Rallis, M. Zohrabi, R. Siemering, B. Jochim, P. R. Andrews, U. Ablikim, B. Gaire, S. De, K. D. Carnes, B. Bergues, R. de Vivie-Riedle, M. F. Kling, and I. Ben-Itzhak, *Nat. Commun.* **4**, 2895 (2013).
 - [16] H. Ibrahim, B. Wales, S. Beaulieu, B. E. Schmidt, N. Thiré, E. P. Fowe, É. Bisson, C. T. Hebeisen, V. Wanie, M. Giguère, J.-C. Kieffer, M. Spanner, A. D. Bandrauk, J. Sanderson, M. S. Schuurman, and F. Légaré, *Nat. Commun.* **5**, 4422 (2014).
 - [17] X. Gong, Q. Song, Q. Ji, K. Lin, H. Pan, J. Ding, H. Zeng, and J. Wu, *Phys. Rev. Lett.* **114**, 163001 (2015).
 - [18] S. Xu, X. L. Zhu, W. T. Feng, D. L. Guo, Q. Zhao, S. Yan, P. Zhang, D. M. Zhao, Y. Gao, S. F. Zhang, J. Yang, and X. Ma, *Phys. Rev. A* **97**, 062701 (2018).

- [19] N. Neumann, D. Hant, L. P. H. Schmidt, J. Titze, T. Jahnke, A. Czasch, M. S. Schöffler, K. Kreidi, O. Jagutzki, H. Schmidt-Bocking, and R. Dörner, *Phys. Rev. Lett.* **104**, 103201 (2010).
- [20] C. Wu, C. Wu, D. Song, H. Su, Y. Yang, Z. Wu, X. Liu, H. Liu, M. Li, Y. Deng, Y. Liu, L. Y. Peng, H. Jiang, and Q. Gong, *Phys. Rev. Lett.* **110**, 103601 (2013).
- [21] E. Wang, X. Shan, Z. Shen, M. Gong, Y. Tang, Y. Pan, K.-C. Lau, and X. Chen, *Phys. Rev. A* **91**, 052711 (2015).
- [22] J. Rajput, T. Severt, B. Berry, B. Jochim, P. Feizollah, B. Kaderiya, M. Zohrabi, U. Ablikim, F. Ziaee, P. Kanaka Raju P., D. Rolles, A. Rudenko, K. D. Carnes, B. D. Esry, and I. Ben-Itzhak, *Phys. Rev. Lett.* **120**, 103001 (2018).
- [23] X. Wang, Y. Zhang, D. Lu, G. C. Lu, B. Wei, B. H. Zhang, Y. J. Tang, R. Hutton, and Y. Zou, *Phys. Rev. A* **90**, 062705 (2014).
- [24] Y. Zhang, T. Jiang, L. Wei, D. Luo, X. Wang, W. Yu, R. Hutton, Y. Zou, and B. Wei, *Phys. Rev. A* **97**, 022703 (2018).
- [25] B. Wei, Y. Zhang, X. Wang, D. Lu, G. C. Lu, B. H. Zhang, Y. J. Tang, R. Hutton, and Y. Zou, *J. Chem. Phys.* **140**, 124303 (2014).
- [26] Y. Zhang, X. Wang, D. Lu, B. Wei, B. H. Zhang, Y. J. Tang, R. Hutton, and Y. Zou, *Nucl. Instrum. Methods Phys. Res., Sect. B* **337**, 39 (2014).
- [27] Y. Zhang, X. Wang, L. F. Zhu, D. Lu, R. Hutton, Y. Zou, and B. Wei, *J. Phys. B: At., Mol. Opt. Phys.* **50**, 205202 (2017).
- [28] Y. Zhang, B. Wang, L. Wei, T. Jiang, W. Yu, R. Hutton, Y. Zou, L. Chen, and B. Wei, *J. Chem. Phys.* **150**, 204303 (2019).
- [29] S. Xu, H. Zhao, X. Zhu, D. Guo, W. Feng, K. C. Lau, and X. Ma, *Phys. Chem. Chem. Phys.* **20**, 27725 (2018).
- [30] R. H. Dalitz, *London, Edinburgh Dublin Philos. Mag. J. Sci.* **44**, 1068 (2009).
- [31] P. Bhatt, T. Sairam, A. Kumar, H. Kumar, and C. P. Safvan, *Phys. Rev. A* **96**, 022710 (2017).
- [32] M. Alagia, C. Callegari, P. Candori, S. Falcinelli, F. Pirani, R. Richter, S. Stranges, and F. Vecchiocattivi, *J. Chem. Phys.* **136**, 204302 (2012).
- [33] C. Maul and K.-H. Gericke, *Int. Rev. Phys. Chem.* **16**, 1 (1997).
- [34] W. Yu, C. -Z. Gao, T. Jiang, Y. Zou, J. -G. Wang, Y. Wu, and B. Wei, *J. Chem. Phys.* **150**, 124304 (2019).